Available online at www.sciencedirect.com
ScienceDirect
Journal of Sound and Vibration 312 (2008) 55–73
JOURNAL OF SOUND AND VIBRATION
www.elsevier.com/locate/jsvi

Free vibration of laminated cylindrical shells with a circular cutout

A.L. Poore, A. Barut, E. Madenci*

Department of Aerospace and Mechanical Engineering, The University of Arizona, Tucson, AZ 85721, USA

Received 2 March 2007; received in revised form 5 October 2007; accepted 16 October 2007
Available online 3 December 2007

Abstract

A semi-analytical solution method is presented for determining the natural frequencies and mode shapes of laminated cylindrical shells containing a circular cutout. The method utilizes Hamilton's principle to obtain the governing equations for the vibration response of the shell. In the derivation of governing equations, Lagrange multipliers are employed to relax the kinematic admissibility requirements on the displacement representations through the use of idealized elastic edge restraints. Specifying appropriate stiffness values for the elastic extensional and rotational edge restraints (springs) allows the imposition of the kinematic boundary conditions in an indirect manner, which enables the use of a broader set of functions for representing the displacement fields. The natural frequencies and the corresponding modes of the shell are determined by transforming the governing equations into a matrix eigenvalue problem. The present semi-analytical solution method accurately predicts the natural frequency and vibration modes of the shells with a cutout. The focus of this study is to investigate the effects of varying cutout size, shell radius, and laminate layup, as well as the effects of two types of boundary conditions on the shell vibration response. Selected results of the parametric studies are presented for several geometric parameters to demonstrate that this semi-analytical approach is a powerful means for optimizing design parameters.

1. Introduction

Composite cylindrical shells can be easily manufactured with desired structural stiffness properties. Depending on the application, the shells may contain cutouts to be used, for example, as access panels or ventilation holes. These cutouts can change the static and dynamic behaviors of the shell. For ease of solution, a designer may perform an analysis that neglects the presence of cutouts. However, this can potentially lead to undesirable consequences, such as resonance. When resonance occurs, the shell can experience very large oscillations that may cause high stresses and strains, potentially leading to failure. Also, sensitive electronic components, such as connectors or circuit boards, located on the inner surface of shells may experience failure due to shell resonance.

The vibration response of composite cylindrical shells has been investigated extensively by a number of researchers, but many of these studies were completed without considering a cutout. Among these previous

*Corresponding author.
E-mail address: madenci@email.arizona.edu (E. Madenci).

0022-460X/$ - see front matter © 2007 Elsevier Ltd. All rights reserved.
doi:10.1016/j.jsv.2007.10.025

studies employing the finite element method, Lakshminarayana [1] focused on the effects of material anisotropy on the vibration frequency, Ramesh and Ganesan [2] developed a finite element formulation based on a discrete layer theory to perform vibration analysis, and Sun et al. [3] used nine-noded isoparametric quadratic finite elements based on Sander's first-order shear deformable shell theory to study the fundamental frequencies of cylindrical composite shells.

Without resorting to the finite element method, Soldatos [4] studied the effect of coupling between bending and extension of composites on the vibration frequency by using Donnell-type equations of motion in conjunction with Galerkin's method. Considering the equations of motion based on Love's first approximation of the classical shell theory, Shu and Du [5] utilized the global method of generalized differential quadrature to investigate the free vibration of laminated cylindrical shells. Zhang [6] extended a previously developed wave propagation approach to analyze the natural frequencies of cross-ply laminated cylindrical shells. Moussaoui et al. [7] investigated the vibrations of infinitely long circular cylindrical composite shells and their nonlinear behavior by using Hamilton's principle with spectral analysis extended for shell-type structures. The point collocation method, along with spline function approximations, was used by Viswanathan and Navaneethakrishnan [8] to study the free vibration of thin circular cylindrical composite shells.

A few analytical studies provided closed-form solutions to the free vibration of noncircular shells. Narisawa [9] studied the free vibration response of composite cylindrical shells using equivalent curvatures to estimate the curvature of the mid-plane of the shell and equivalent transverse shear stiffness for estimation of the rotation of the transverse cross section. Hufenbach et al. [10] investigated the damped vibration of slender cylindrical composite shells by developing an analytical model analogous to the Timoshenko beam theory.

None of these previous studies on the vibration response of laminated cylindrical shells included the presence of a cutout. There are only a few studies based on the finite element method that do consider the presence of a cutout. Among these studies, Bicos and Springer [11,12] investigated the vibrations of laminated composite plates and shells with or without cutouts while including the effects of damping. Also, Hu and Tsai [13] considered the optimization of shell layups to maximize the fundamental frequencies.

Although the natural frequency of a composite cylindrical shell with a cutout can be evaluated by using the finite element method, the predictions can be inconsistent, depending on the element type considered in the analysis. Therefore, the objective of this study is to develop a semi-analytical method for the free vibration response of laminated cylindrical shells with cutouts and to evaluate the effect of cutout size, shell radius, and laminate layup on the natural frequencies.

2. Problem statement

This study considers circular cylindrical shells with orthotropic layers containing a circular cutout, as shown in Fig. 1. The shell is of constant thickness and considered thin, i.e., the thickness is much smaller than the other dimensions of the shell. The radius of the circular cutout is never larger than half the shell radius, and the length of the shell is always at least twice the shell radius.

As shown in Fig. 1, a Cartesian coordinate system is located at the end of the shell, and its x-axis coincides with the longitudinal axis of the shell. A curvilinear coordinate system is attached to the mid-surface of the shell. The longitudinal coordinate is denoted by s_1, the circumferential by s_2, and the normal-to-the surface by s_3. The corresponding base vectors, $\{\mathbf{e}_1, \mathbf{e}_2, \mathbf{e}_3\}$, are also shown in Fig. 1.

The cutout is located at the shell mid-length, as shown in Fig. 1. In order to describe the cutout, the shell is viewed as flat when cut longitudinally opposite the cutout so that it appears as in Fig. 2. In this flat plane, the cutout is defined in the shape of a circular hole with radius a, and (s_1, s_2) axes become a Cartesian coordinate system. Also, a local Cartesian coordinate system (x_1, x_2), which is parallel to (s_1, s_2), is placed at the center of the circular cutout as shown in Fig. 2.

As shown in Fig. 1, the internal and external edge boundaries of the shell are decomposed into three parts

$$\Gamma = \Gamma_{(1)} + \Gamma_{(2)} + \Gamma_{(3)}, \tag{1}$$

where $\Gamma_{(1)}$ and $\Gamma_{(2)}$ represent the external shell edges, and $\Gamma_{(3)}$ represents the internal edge around the cutout. Unit normal vectors to the edges are expressed as $\mathbf{n}$.

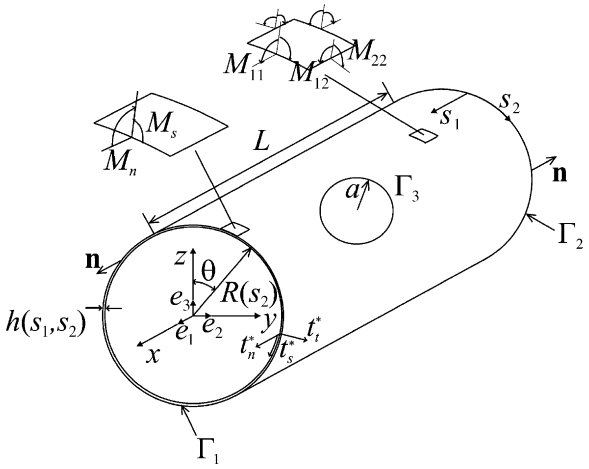

Fig. 1. Geometry and coordinate systems for a cylindrical shell.

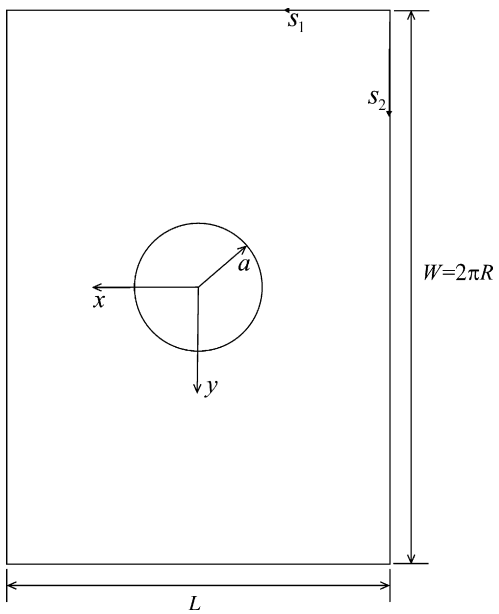

Fig. 2. Geometry of the cutout on the s_1–s_2 plane.

The shell edges can have one of two different types of simply supported boundary conditions, namely, simply supported 2 (SS2) or simply supported 3 (SS3). The difference between these boundary conditions is that SS3 boundary conditions enforce a restraint against axial expansion of the shell edge whereas SS2 boundary conditions allow the shell edges to expand freely. The displacements and rotations that are restrained for these two types of boundary conditions are shown in Fig. 3.

The shells are made of K layers which are specially orthotropic. Each layer has an orientation of ϑ_k from the s_1-axis. The material properties of each layer are the elastic moduli, E_{11} and E_{22}, the shear modulus, G_{12}, Poisson's ratio v_{12}, and the mass density, ρ. The subscripts 1 and 2 denote the longitudinal (fiber) and transverse material directions of each ply, respectively.

In studying the effects of a cutout on the natural frequencies of composite cylindrical shells, (1) the cutout radius is increased for specified shell radius and material layup, (2) the radius of the shell is increased for

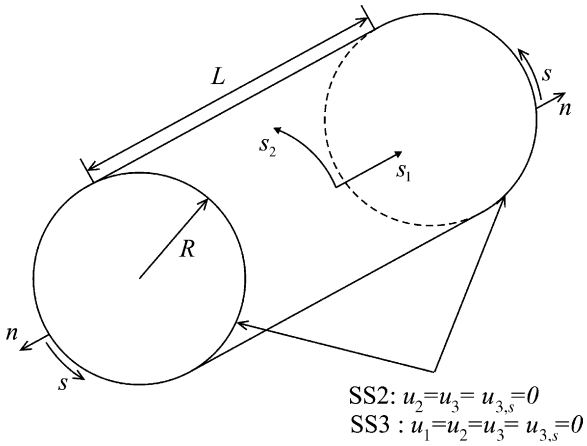

Fig. 3. Simply supported boundary conditions of types SS2 (free to axial movement) and SS3 (restrained to axial movement) applied along the edges of the shell.

specified cutout radius and material layup, and (3) the number of plies in the shell is increased for specified geometry.

3. Problem formulation

3.1. Overview

A semi-analytical vibration analysis, an extension of the static analysis by Oterkus et al. [14] are developed based on Hamilton's principle. The method utilizes global (polynomials) and local (complex variable) functions to represent the mid-surface displacements. Global functions are used over the entire shell to capture the overall shell displacement and local functions are used only in a specified region near the cutout. Fourier series are used for the global functions and Laurent series for the local functions, as they are convergent and more representative of steep field variations in areas around a cutout. The edges of the shell are supported by extensional and rotational springs, and zero-valued boundary conditions are enforced by assigning a spring stiffness that is much larger than the stiffness of the material.

The equations of motion are derived by using Hamilton's principle in which the total potential energy of the system includes the elastic strain energy of the shell, the strain energy of the springs on the edges, and the potential energy arising from the constraints on the shell. Lagrange multipliers are used to impose constraints on the global and local functions in order to uniquely define the displacement field representations.

3.2. Application of boundary conditions

The boundary conditions are enforced through springs along the shell edges. Five different springs are used, as shown in Fig. 4: three extensional for the axial, tangential, and normal boundary displacements, and two rotational for the bending and twisting boundary conditions.

A spring stiffness much higher than the stiffness of the shell is specified in order to restrain the motion of a shell edge with zero displacement. A spring stiffness of zero is specified in order to simulate a traction-free edge. In order to achieve SS2 and SS3 boundary conditions using the elastic edge restraints, the extensional and rotational springs are specified with spring constants that are, respectively, 10^4 times the diagonal sums of in-plane and bending stiffness matrices of the shell as given in Eq. (24c) in Section 3.5. Hence, the use of springs on the shell edges to enforce boundary conditions relaxes the kinematic admissibility requirements on the functions that are assumed for the displacement fields.

The extensional springs restricting the edge displacements, u_n, u_s, and u_t, have stiffness values of S_n, S_s, and S_t, where the subscript n denotes the axial direction, s denotes the tangential direction, and t denotes the

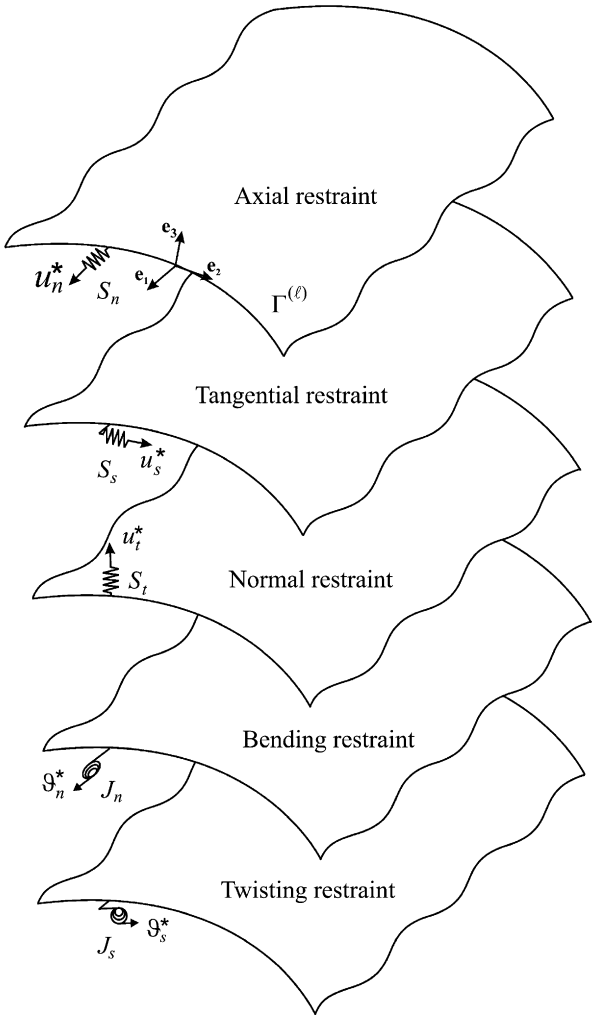

Fig. 4. Elastic spring restraints on shell edges.

normal direction. The edge rotations ϑ_n and ϑ_s are also restricted by rotational springs with stiffnesses of J_n and J_s, where the subscript n represents rotation about an axis tangent to the shell edge and s represents rotation about an axis normal to the shell edge.

3.3. Kinematics and stress–strain relations

3.3.1. Displacement of a point in the shell

The kinematic relations are derived based on the assumptions of the Love–Kirchhoff classical thin-shell theory. The displacements of a point on the shell mid-surface are denoted by $u_1(s_1, s_2)$, $u_2(s_1, s_2)$, and $u_3(s_1, s_2)$, where u_1 is the axial displacement, u_2 is the circumferential (tangential) displacement, and u_3 is the normal (normal-to-mid-surface) displacement. These are related to the displacement of any point in the shell through the following equations:

$$U_1(s_1, s_2, s_3) = u_1(s_1, s_2) - s_3 u_{3,1}(s_1, s_2), \tag{2a}$$

$$U_2(s_1, s_2, s_3) = u_2(s_1, s_2) - s_3\left(u_{3,2}(s_1, s_2) - \tfrac{1}{R}u_2(s_1, s_2)\right), \tag{2b}$$

$$U_3(s_1, s_2, s_3) = u_3(s_1, s_2), \tag{2c}$$

where a subscript after a comma denotes partial differentiation. The terms with $1/R$ account for the change in curvature of the s_2-axis in the circumferential direction.

3.3.2. Displacement field representation

The mid-surface displacement fields are defined as a combination of rigid-body modes, u_{Ri}, global functions, $\bar{u}_i$, and local functions, $\bar{\bar{u}}_i$, as follows:

$$u_i = u_{Ri} + \bar{u}_i + \bar{\bar{u}}_i \quad (i = 1, 2, 3). \tag{3}$$

Rigid-body mode: The rigid-body modes capture the overall translation and rotation of the shell and cause no strain within the material or changes in the shell curvature and twist. They are included in the displacement field representation to allow for all possible motions of the shell. Imposition of SS2 or SS3 boundary conditions to the shell edges partially or fully eliminates the rigid-body motion of the shell. If not fully eliminated, it is suppressed explicitly by introducing Lagrange multipliers. The rigid-body modes can be expressed in the form

$$u_{Ri} = \mathbf{V}_{Ri}^{\mathrm{T}} \boldsymbol{\alpha}_R \quad (i = 1, 2, 3), \tag{4}$$

where $\boldsymbol{\alpha}_R$ is a vector of time-dependent unknown coefficients and $\mathbf{V}_{Ri}^{\mathrm{T}}$ represents the known vectors.

Global functions: The global functions account for the overall deformation of the shell and are expressed in terms of trigonometric expansions. They can be written in compact vector form as

$$\bar{u}_i(s_1, s_2) = \bar{\mathbf{V}}_i^{\mathrm{T}} \mathbf{c}_i \quad (i = 1, 2, 3), \tag{5}$$

where $\mathbf{c}_i$ is a vector of unknown, real-valued, and time-dependent coefficients and $\bar{\mathbf{V}}_i^{\mathrm{T}}$ represents known vectors.

Local functions: Laurent series are used as local functions because they are analytic and convergent in regions with a circular cutout and help in capturing the steep variations of deformations around the cutout. They can be expressed in compact form as

$$\bar{\bar{u}}_i = \bar{\bar{\mathbf{V}}}_i^{\mathrm{T}} \boldsymbol{\alpha} \quad (i = 1, 2) \tag{6a}$$

and

$$\bar{\bar{u}}_3 = \bar{\bar{\mathbf{V}}}_3^{\mathrm{T}} \boldsymbol{\beta}. \tag{6b}$$

The explicit definitions of the time-dependent unknown vectors, $\boldsymbol{\alpha}_R$, $\mathbf{c}_i$, $\boldsymbol{\alpha}$, and $\boldsymbol{\beta}$, and the known vectors, $\mathbf{V}_{Ri}^{\mathrm{T}}$, $\bar{\mathbf{V}}_i^{\mathrm{T}}$, and $\bar{\bar{\mathbf{V}}}_i^{\mathrm{T}}$ $(i = 1,2,3)$, are given by Oterkus et al. [14].

Vector form of the mid-surface displacement field: Combining Eqs. (4), (5), (6a) and (6b), the mid-surface displacement field representation can be written as

$$u_i = \mathbf{V}_i^{\mathrm{T}} \mathbf{q} \quad (i = 1, 2, 3), \tag{7}$$

where $\mathbf{q}$ is the vector containing all of the unknown time-dependent displacement coefficients defined as

$$\mathbf{q}^{\mathrm{T}} = \{\boldsymbol{\alpha}_R^{\mathrm{T}}, \mathbf{c}_1^{\mathrm{T}}, \mathbf{c}_2^{\mathrm{T}}, \mathbf{c}_3^{\mathrm{T}}, \boldsymbol{\alpha}^{\mathrm{T}}, \boldsymbol{\beta}^{\mathrm{T}}\} \tag{8}$$

and $\mathbf{V}_i^{\mathrm{T}}$ contains the vector functions associated with the rigid-body modes, the global functions, and the local functions and is defined as

$$\mathbf{V}_1^{\mathrm{T}} = \{\mathbf{V}_{R1}^{\mathrm{T}}, \bar{\mathbf{V}}_1^{\mathrm{T}}, \bar{\mathbf{0}}^{\mathrm{T}}, \bar{\mathbf{0}}^{\mathrm{T}}, \bar{\bar{\mathbf{V}}}_1^{\mathrm{T}}, \bar{\bar{\mathbf{0}}}^{\mathrm{T}}\}, \tag{9a}$$

$$\mathbf{V}_2^{\mathrm{T}} = \{\mathbf{V}_{R2}^{\mathrm{T}}, \bar{\mathbf{0}}^{\mathrm{T}}, \bar{\mathbf{V}}_2^{\mathrm{T}}, \bar{\mathbf{0}}^{\mathrm{T}}, \bar{\bar{\mathbf{V}}}_2^{\mathrm{T}}, \bar{\bar{\mathbf{0}}}^{\mathrm{T}}\}, \tag{9b}$$

$$\mathbf{V}_3^{\mathrm{T}} = \{\mathbf{V}_{R3}^{\mathrm{T}}, \bar{\mathbf{0}}^{\mathrm{T}}, \bar{\mathbf{0}}^{\mathrm{T}}, \bar{\mathbf{V}}_3^{\mathrm{T}}, \bar{\bar{\mathbf{0}}}^{\mathrm{T}}, \bar{\bar{\mathbf{V}}}_3^{\mathrm{T}}\}, \tag{9c}$$

where

$$\bar{\mathbf{0}}^{\mathrm{T}} = \{0, 0, 0, \ldots, 0\} \text{ of order}[(M + 1)(M + 1/2)], \tag{10a}$$

$$\bar{\mathbf{0}}^{\mathrm{T}} = \{0, 0, \ldots, 0\} \text{ of order } 8N, \tag{10b}$$

where M and N represent the number of terms retained in the global and local (complex) series employed in the model. The explicit forms of these series are given by Oterkus et al. [14].

3.4. Boundary displacements

A vector representation similar to that of Eq. (7) is utilized for the displacements and rotations of points along the shell's exterior boundaries, i.e., $\Gamma_{(1)}$ and $\Gamma_{(2)}$. This representation is given by

$$\mathbf{u}_{\Gamma} = \mathbf{B}\,\mathbf{q}, \tag{11}$$

where $\mathbf{u}_{\Gamma}$ consists of the mid-surface boundary displacements that are normal, u_n, tangent, u_s, and transverse, u_t, to a shell edge and the mid-surface boundary rotations, ϑ_n, about the axis tangent to a shell edge. In vector form, $\mathbf{u}_{\Gamma}$ is expressed as

$$\mathbf{u}_{\Gamma}^{\mathrm{T}} = \{u_n, u_s, u_t, \vartheta_n\} \tag{12}$$

and $\mathbf{B}$ is a known matrix of coefficients defined as

$$\mathbf{B} = \begin{bmatrix} \mathbf{u}_n^{\mathrm{T}} \\ \mathbf{u}_s^{\mathrm{T}} \\ \mathbf{u}_t^{\mathrm{T}} \\ \boldsymbol{\theta}_n^{\mathrm{T}} \end{bmatrix}, \tag{13}$$

where the known sub-vectors are given by

$$\mathbf{u}_n^{\mathrm{T}} = (\mathbf{n} \cdot \mathbf{e}_1)\mathbf{V}_1, \tag{14a}$$

$$\mathbf{u}_s^{\mathrm{T}} = [(\mathbf{e}_3 \times \mathbf{n}) \cdot \mathbf{e}_2]\mathbf{V}_2, \tag{14b}$$

$$\mathbf{u}_t^{\mathrm{T}} = \mathbf{V}_3^{\mathrm{T}}, \tag{14c}$$

$$\boldsymbol{\theta}_n^{\mathrm{T}} = (\mathbf{n} \cdot \mathbf{e}_1)\mathbf{V}_{3,1}^{\mathrm{T}}. \tag{14d}$$

3.5. Strain and curvature

The linear membrane–strain displacement equations and bending–strain displacement equations are expressed as

$$\boldsymbol{\varepsilon} = \begin{Bmatrix} \varepsilon_{11} \\ \varepsilon_{22} \\ \gamma_{12} \end{Bmatrix} = \begin{Bmatrix} u_{1,1} \\ \left(u_{2,2} + \frac{1}{R}u_3\right) \\ (u_{1,2} + u_{2,1}) \end{Bmatrix}, \tag{15a}$$

$$\boldsymbol{\kappa} = \begin{Bmatrix} \kappa_{11} \\ \kappa_{22} \\ \kappa_{12} \end{Bmatrix} = \begin{Bmatrix} -u_{3,11} \\ -\left(u_{3,22} - \left(\frac{u_2}{R}\right)_{,2}\right) \\ -2\left(u_{3,12} - \frac{1}{R}u_{2,1}\right) \end{Bmatrix}, \tag{15b}$$

where the terms with $1/R$ account for the change in curvature of the shell in the circumferential direction. In this study, $1/R$ remains uniform with constant shell radius.

By substituting Eq. (7) into Eqs. (15a) and (15b), these equations can be rewritten in terms of the generalized coordinate $\mathbf{q}$ as

$$\varepsilon = \mathbf{L}_{\varepsilon}\mathbf{q}, \tag{16a}$$

$$\boldsymbol{\kappa} = \mathbf{L}_{\kappa}\mathbf{q}, \tag{16b}$$

where the strain-coefficient matrices $\mathbf{L}_{\varepsilon}$ and $\mathbf{L}_{\kappa}$ are defined as

$$\mathbf{L}_{\varepsilon} = \begin{bmatrix} \mathbf{V}_{1,1}^{\mathrm{T}} \\ \mathbf{V}_{2,2}^{\mathrm{T}} + \frac{1}{R}\mathbf{V}_{3}^{\mathrm{T}} \\ \mathbf{V}_{1,2}^{\mathrm{T}} + \mathbf{V}_{2,1}^{\mathrm{T}} \end{bmatrix}, \tag{17a}$$

$$\mathbf{L}_{\kappa} = \begin{bmatrix} -\mathbf{V}_{3,11}^{\mathrm{T}} \\ -\mathbf{V}_{3,22}^{\mathrm{T}} + \frac{1}{R}\mathbf{V}_{2,2}^{\mathrm{T}} \\ -2\mathbf{V}_{3,12}^{\mathrm{T}} + \frac{2}{R}\mathbf{V}_{2,1}^{\mathrm{T}} \end{bmatrix}. \tag{17b}$$

These equations can be combined into an overall strain-coefficient matrix $\mathbf{L}$ as

$$\mathbf{L}^{\mathrm{T}} = [\,\mathbf{L}_{\varepsilon}^{\mathrm{T}} \quad \mathbf{L}_{\kappa}^{\mathrm{T}}\,]. \tag{18}$$

3.6. Stress–strain relations

Based on the classical laminated shell theory, the relationships between the membrane and bending stress resultants and the membrane and bending strains are given by

$$\mathbf{N} = \mathbf{A}\,\boldsymbol{\varepsilon} + \mathbf{B}\,\boldsymbol{\kappa}, \tag{19a}$$

$$\mathbf{M} = \mathbf{B}\,\boldsymbol{\varepsilon} + \mathbf{D}\,\boldsymbol{\kappa}, \tag{19b}$$

with $\mathbf{N}$ and $\mathbf{M}$ defined as

$$\mathbf{N}^{\mathrm{T}} = \{N_{11}, N_{22}, N_{12}\}, \tag{20a}$$

$$\mathbf{M}^{\mathrm{T}} = \{M_{11}, M_{22}, M_{12}\}, \tag{20b}$$

and from classical shell theory

$$N_{ij} = \int_{s_3} \sigma_{ij}\,\mathrm{d}s_3, \tag{21}$$

$$M_{ij} = \int_{s_3} \sigma_{ij} s_3\,\mathrm{d}s_3, \tag{22}$$

where σ_{ij} $(i, j = 1,2)$ are the membrane stresses in the shell.

Combining Eqs. (19a) and (19b) leads to

$$\mathbf{s} = \mathbf{C}\mathbf{e}, \tag{23}$$

with

$$\mathbf{s}^{\mathrm{T}} = \{\mathbf{N}^{\mathrm{T}}, \mathbf{M}^{\mathrm{T}}\}, \tag{24a}$$

$$\mathbf{e}^{\mathrm{T}} = \{\boldsymbol{\varepsilon}^{\mathrm{T}}, \boldsymbol{\kappa}^{\mathrm{T}}\}, \tag{24b}$$

$$\mathbf{C} = \begin{bmatrix} \mathbf{A} & \mathbf{B} \\ \mathbf{B} & \mathbf{D} \end{bmatrix}, \tag{24c}$$

where $\mathbf{A}$ represents the extensional stiffness matrix, $\mathbf{B}$ represents the extension-bending coupling matrix, and $\mathbf{D}$ represents the bending stiffness matrix. Furthermore, Eq. (24b) can be rewritten in terms of $\mathbf{L}$ and $\mathbf{q}$ as

$$\mathbf{e} = \mathbf{L}\,\mathbf{q}. \tag{25}$$

Consequently, the stress resultants can be expressed in terms of the generalized coordinates, $\mathbf{q}$, by substituting Eq. (25) into Eq. (23) as

$$\mathbf{s} = \mathbf{C}\,\mathbf{L}\,\mathbf{q}. \tag{26}$$

4. Derivation of governing equations

The governing equations for free vibration of the shell are derived by using Hamilton's principle given by

$$\int_{t_1}^{t_2} (\delta T - \delta\pi)\,\mathrm{d}t = 0, \tag{27}$$

where T is the kinetic energy of the system and π represents the total potential energy. In accordance with Hamilton's principle, the difference between the time integrals of the first variations of the kinetic and potential energies along any arbitrary time interval, $t_1 \leqslant t \leqslant t_2$, must be stationary for dynamic equilibrium to exist. The variational operator is defined by δ. The derivations of the total potential energy, π, and the kinetic energy, T, terms are given in the subsequent sections.

4.1. Total potential energy of the shell

The total potential energy of the shell, π, consists of the elastic strain energy of the shell and the elastic springs along the shell edges, and the potential energy from the constraint reactions. It can be expressed as

$$\pi(\mathbf{q}) = U(\mathbf{q}) + \Omega(\mathbf{q}) + W(\mathbf{q}, \boldsymbol{\lambda}), \tag{28}$$

where U represents the strain energy of the shell, Ω represents the strain energy of the springs, and W represents the potential energy from the constraint forces. The symbol $\mathbf{q}$ is the vector of generalized coordinates defined earlier, and $\boldsymbol{\lambda}$ is a vector of unknown Lagrange multipliers. Both $\mathbf{q}$ and $\boldsymbol{\lambda}$ are unknown time-dependent vectors. Derivations for the expressions for U, Ω, and W are given by Oterkus et al. [14]. Their final matrix forms are

$$U(\mathbf{q}) = \tfrac{1}{2}\mathbf{q}^{\mathrm{T}}\mathbf{k}_{qq}\mathbf{q}, \tag{29a}$$

$$\Omega(\mathbf{q}) = \tfrac{1}{2}\mathbf{q}^{\mathrm{T}}\mathbf{S}_{qq}\mathbf{q}, \tag{29b}$$

$$W(\mathbf{q}, \boldsymbol{\lambda}) = \boldsymbol{\lambda}^{\mathrm{T}}\mathbf{G}\,\mathbf{q} = 0, \tag{29c}$$

where $\mathbf{k}_{qq}$ represents the stiffness matrix of the shell, $\mathbf{S}_{qq}$ is associated with the stiffness of the springs restraining the deformation of the shell edges, and $\mathbf{G}$ is the constraint coefficient matrix, all of which are also explicitly defined by Oterkus et al. [14].

Substituting the expressions for U, Ω, and W in Eq. (28) with their respective forms in Eq. (29) results in the total potential of the shell in matrix form

$$\pi(\mathbf{q}) = \mathbf{q}^{\mathrm{T}}(\tfrac{1}{2}\mathbf{k}_{qq}\mathbf{q} + \tfrac{1}{2}\mathbf{S}_{qq}\mathbf{q}) + \boldsymbol{\lambda}^{\mathrm{T}}\mathbf{G}\,\mathbf{q}, \tag{30}$$

whose first variation is obtained as

$$\delta\pi = \delta\mathbf{q}^{\mathrm{T}}[\mathbf{k}_{qq}\mathbf{q} + \mathbf{S}_{qq}\mathbf{q} + \mathbf{G}^{\mathrm{T}}\boldsymbol{\lambda}] + \delta\boldsymbol{\lambda}^{\mathrm{T}}\mathbf{G}\,\mathbf{q}. \tag{31}$$

4.2. Kinetic energy of the shell

The kinetic energy of the shell is given by

$$T = \frac{1}{2}\sum_{i=1}^{3}\int_V \rho_i \dot{U}_i^2\,\mathrm{d}V, \tag{32}$$

where ρ_i $(i = 1, 2, 3)$ represents the material density in the s_i directions, respectively, and $\dot{U}_i$ are the time derivatives of the displacements at a generic point in the shell whose volume is V. Its first variation is obtained as

$$\delta T = \sum_{i=1}^{3} \int_V \rho_i \dot{U}_i \delta \dot{U}_i \, \mathrm{d}V. \tag{33}$$

After substituting from Eq. (2) into Eq. (7) and performing differentiation with respect to time, the first variation of the time derivative of the displacement components at a generic point can be expressed as

$$\delta \dot{U}_1 = (\mathbf{V}_1^{\mathrm{T}} - s_3 \mathbf{V}_{3,1}^{\mathrm{T}}) \delta \dot{\mathbf{q}}, \tag{34a}$$

$$\delta \dot{U}_2 = \left(\mathbf{V}_2^{\mathrm{T}} - s_3 \left(\mathbf{V}_{3,2}^{\mathrm{T}} - \tfrac{1}{R} \mathbf{V}_2^{\mathrm{T}} \right) \right) \delta \dot{\mathbf{q}}, \tag{34b}$$

$$\delta \dot{U}_3 = \mathbf{V}_3^{\mathrm{T}} \delta \dot{\mathbf{q}}. \tag{34c}$$

With these expressions, the variation of the kinetic energy can be rewritten in compact form as

$$\delta T = \delta \dot{\mathbf{q}}^{\mathrm{T}} \mathbf{M} \dot{\mathbf{q}}, \tag{35}$$

with

$$\begin{aligned} \mathbf{M} = & \int_V \rho_1 (\mathbf{V}_1 - s_3 \mathbf{V}_{3,1})(\mathbf{V}_1^{\mathrm{T}} - s_3 \mathbf{V}_{3,1}^{\mathrm{T}}) \, \mathrm{d}V \\ & + \int_V \rho_2 \left(\mathbf{V}_2 - s_3 \left(\mathbf{V}_{3,2} - \frac{1}{R} \mathbf{V}_2 \right) \right) \left(\mathbf{V}_2^{\mathrm{T}} - s_3 \left(\mathbf{V}_{3,2}^{\mathrm{T}} - \frac{1}{R} \mathbf{V}_2^{\mathrm{T}} \right) \right) \mathrm{d}V \\ & + \int_V \rho_3 \mathbf{V}_3 \mathbf{V}_3^{\mathrm{T}} \, \mathrm{d}V, \end{aligned} \tag{36}$$

where $\mathbf{M}$ represents the mass matrix of the shell.

Substituting the variations of the kinetic energy and potential energy into Hamilton's principle and integrating the integral involving time derivatives of the generalized coordinates through integration by parts result in

$$\int_{t_1}^{t_2} -\delta \mathbf{q}^{\mathrm{T}} (\mathbf{M} \ddot{\mathbf{q}} - \delta \mathbf{q}^{\mathrm{T}} [\mathbf{k}_{qq} \mathbf{q} + \mathbf{S}_{qq} \mathbf{q} + \mathbf{G}^{\mathrm{T}} \boldsymbol{\lambda}]) \, \mathrm{d}t - \int_{t_1}^{t_2} \delta \boldsymbol{\lambda}^{\mathrm{T}} \mathbf{G} \, \mathbf{q} \, \mathrm{d}t = 0, \tag{37}$$

Since $\delta \mathbf{q}$ and $\delta \boldsymbol{\lambda}$ are arbitrary first variations of the solution vectors $\mathbf{q}$ and $\boldsymbol{\lambda}$, this equation can only be satisfied if the coefficients of $\delta \mathbf{q}$ and $\delta \boldsymbol{\lambda}$ vanish, thus leading to

$$\mathbf{M} \ddot{\mathbf{q}} + \mathbf{k}_{qq} \mathbf{q} + \mathbf{S}_{qq} \mathbf{q} + \mathbf{G}^{\mathrm{T}} \boldsymbol{\lambda} = \mathbf{0}, \tag{38a}$$

$$\mathbf{G} \mathbf{q} = \mathbf{0}. \tag{38b}$$

These two equations can be rewritten in matrix form as

$$\begin{bmatrix} \mathbf{M} & \mathbf{0} \\ \mathbf{0} & \mathbf{0} \end{bmatrix} \begin{Bmatrix} \ddot{\mathbf{q}} \\ \boldsymbol{\lambda} \end{Bmatrix} + \begin{bmatrix} \mathbf{k}_{qq} + \mathbf{S}_{qq} & \mathbf{G}^{\mathrm{T}} \\ \mathbf{G} & \mathbf{0} \end{bmatrix} \begin{Bmatrix} \mathbf{q} \\ \boldsymbol{\lambda} \end{Bmatrix} = \begin{Bmatrix} \mathbf{0} \\ \mathbf{0} \end{Bmatrix}. \tag{39}$$

In order to obtain a solution for free vibration of the shell, the unknown vectors $\mathbf{q}$ and $\boldsymbol{\lambda}$ are represented by harmonic functions in the form

$$\mathbf{q} = \hat{\mathbf{q}} \, \mathrm{e}^{\mathrm{i}\omega t}, \tag{40a}$$

$$\boldsymbol{\lambda} = \hat{\boldsymbol{\lambda}} \, \mathrm{e}^{\mathrm{i}\omega t}, \tag{40b}$$

where $\hat{\mathbf{q}}$ and $\hat{\boldsymbol{\lambda}}$ represent unknown constant coefficients associated with the shell displacement field and the Lagrange multipliers and the parameter to be determined, ω, represents the natural frequency of the shell.

Substituting for $\mathbf{q}$ and $\boldsymbol{\lambda}$ from Eq. (40) into Eq. (39) and rearranging the terms lead to

$$(\bar{\mathbf{K}} - \omega^2\bar{\mathbf{M}})\bar{\mathbf{q}} = \mathbf{0} \tag{41}$$

with

$$\bar{\mathbf{M}} = \begin{bmatrix} \mathbf{M} & \mathbf{0} \\ \mathbf{0} & \mathbf{0} \end{bmatrix}, \tag{42a}$$

$$\bar{\mathbf{K}} = \begin{bmatrix} \mathbf{k}_{qq} + \mathbf{S}_{qq} & \mathbf{G}^{\mathrm{T}} \\ \mathbf{G} & \mathbf{0} \end{bmatrix}, \tag{42b}$$

$$\bar{\mathbf{q}} = \begin{Bmatrix} \hat{\mathbf{q}} \\ \hat{\boldsymbol{\lambda}} \end{Bmatrix}. \tag{42c}$$

Note that the matrices $\mathbf{K}$ and $\mathbf{M}$ are symmetric and definite. However, the matrix $\mathbf{K}$ is not necessarily positive because of the presence of the additional terms in the matrix $\mathbf{G}$ arising from the constraint equations. Therefore, the eigenvalues and eigenvectors of the system are extracted by first pre-multiplying both sides of Eq. (41) by $1/\omega^2\bar{\mathbf{K}}^{-1}$ and rearranging the terms to transform the free vibration problem, Eq. (41), into a more general eigenvalue problem in the form

$$(\mathbf{S}^* - \lambda\mathbf{I})\bar{\mathbf{q}} = \mathbf{0}, \tag{43}$$

where

$$\mathbf{S}^* = \bar{\mathbf{K}}^{-1}\mathbf{M} \quad \text{and} \quad \lambda = 1/\omega^2. \tag{44a, b}$$

The eigenvalues, along with the eigenvectors of the resulting general non-symmetric matrix, $\mathbf{S}^*$, in Eq. (43), are extracted by employing the eigenvalue solver, "rg.f" obtained from the public software, eispack [15]. Finally, the frequencies of all the vibration modes are obtained by inverting all eigenvalues, from which the inverse of the square root of the largest eigenvalue, i.e., $\omega_{\min} = 1/\sqrt{\lambda_{\max}}$, and its corresponding eigenvector yield the smallest natural frequency of and the corresponding mode shape of the cylindrical shell, respectively.

5. Numerical results

The validity of this approach is established by comparison against previously published results based on finite element analysis. The results by Sun et al. [3] without a cutout and of Hu and Tsai [13] with a cutout are compared against the present predictions. In the absence of a cutout, Sun et al. specified the material properties as $E_{11} = 25E_{22}$, $G_{12} = G_{13} = 0.5E_{22}$, $\nu_{12} = 0.25$, and $\rho = 1.0$, with $E_{22} = 1.0 \times 10^6$ psi. The normalized natural frequency is defined as

$$\bar{\omega} = \omega(R^2/h)\sqrt{(\rho/E_{22})}, \tag{45}$$

where ω is the natural frequency, and h, L, and R represent the thickness, length, and radius of the shell, respectively. Their values are specified as $L = 2R$, $h = 0.02R$, and $R = 0.05$ in. For symmetric, anti-symmetric, and angle-ply laminations under both SS2 and SS3 boundary conditions, the comparison of the results between the present analysis and that of Sun et al. given in Table 1 indicates close agreement. Since there is no cutout, the local functions are not included for this analysis. The extent of the Fourier series in the global functions are truncated at 16 terms. This results in a total of 465 degrees of freedom in the governing equations.

In the case of a cutout located at the top of the shell, Hu and Tsai [13] specified the material properties as $E_{11} = 128\,\mathrm{GPa}$, $E_{22} = 11\,\mathrm{GPa}$, $G_{12} = G_{13} = 4.48\,\mathrm{GPa}$, $G_{23} = 1.53\,\mathrm{GPa}$, $\nu_{12} = 0.25$, and $\rho = 1.5 \times 10^3\,\mathrm{kg/m^3}$. The layup is $[\pm\theta^\circ/90^\circ_2/0^\circ]_{2S}$, with $\theta = 46.2^\circ$. The shell is $L = 20\,\mathrm{cm}$ long and has a radius of $R = 10\,\mathrm{cm}$. Each ply is 0.125 mm, thick resulting in a total shell thickness of $h = 2.5\,\mathrm{mm}$. The cutout has a radius of $a = 4\,\mathrm{cm}$.

Because the shell contains a cutout, the Laurent series in the local functions are truncated at 10 terms. The extent of the Fourier series in the global function is truncated at 16 terms. This results in a total of 545 degrees

Table 1
Natural frequencies of cylindrical shells without a cutout

Layup	SS2 boundary condition			SS3 boundary condition		
	Sun et al. [3]	Present study	% Difference	Sun et al. [3]	Present study	% Difference
$[90°/0°]_2$	18.359	18.518	0.864	18.870	19.473	3.198
$[90°/0°]_s$	19.503	19.497	−0.031	20.246	20.237	−0.043
$[\pm 3°]_{15}$	20.681	20.705	0.115	28.184	28.517	1.180
$[\pm 45°]_{15}$	18.765	18.728	−0.196	28.232	28.206	−0.091
$[\pm 60°]_{15}$	17.040	17.425	2.257	26.126	25.909	−0.829

Table 2
Non-dimensionalized natural frequencies, $\bar{\omega}(=\omega(R^2/h)\sqrt{\rho/E_{22}})$, of an anti-symmetric cross-ply cylindrical shell with increasing cutout size under SS2 and SS3 boundary conditions

Normalized cut-out radius, a/R	$\bar{\omega}$ — Boundary conditions	
	SS2	SS3
0	18.518	19.473
0.1	18.526	19.485
0.2	18.551	19.513
0.3	18.435	19.559
0.4	17.897	19.585

of freedom in the governing equations. Under SS3 boundary conditions, Hu and Tsai [13] reported a natural frequency of 2080 Hz, and the present analysis a value of 2115 Hz. The predictions deviate only less than 2.0%, and close agreement also exits for the mode shapes.

In order to investigate the effects of a cutout on the natural frequencies of composite cylindrical shells, three different cases were considered. The first through third cases investigate the effects of increasing cutout size, increasing shell radius, and increasing number of plies in the layup, respectively. Unless otherwise indicated, the material properties are identical to those considered by Sun et al. [3] in their first validation problem.

For all of the cases investigated without a cutout, the Fourier series in the global functions were truncated at 16 terms, resulting in a total of 465 degrees of freedom. When a cutout is present, the Laurent series in the local functions are truncated at 10 terms while the Fourier series in the global functions are truncated at 16 terms. This results in a total of 545 degrees of freedom for the shells containing cutouts. The numbers of terms retained in the Laurent series and the Fourier series were based on a convergence study.

5.1. Effects of increasing cutout size

The first case investigates the effect of cutout size on the modal response of the shell. The shell length, radius, and thickness are respectively specified as $R = 0.05$, $L = 2R$, and $h = 0.02R$ and the cutout size is varied between $a = 0$, $0.1R$, $0.2R$, $0.3R$, and $0.4R$. For this case, non-symmetric and symmetric layups of [90/0/90/0] and [90/0/0/90], respectively, are considered under both SS2 and SS3 boundary conditions.

5.1.1. [90/0/90/0] layup

The natural frequencies corresponding to each cutout size are presented in Table 2 for an anti-symmetric layup of [90/0/90/0] under both SS2 and SS3 boundary conditions. Under SS3 boundary conditions, the frequency increases for increasing cutout size, with a maximum deviation of about 0.57%. Under SS2 boundary conditions, the natural frequency also increases up to the cutout size of $a = 0.2R$, then it decreases

significantly with a deviation of about 3.35% from that of the base line frequency corresponding to no cutout. Under both SS2 and SS3 boundary conditions, the shell always produces three circumferential waves for all cutout sizes, as shown in Figs. 5 and 6.

Under SS2 boundary conditions, the top crest of the wave coincides with the location of the cutout when $a = 0.2R$, whereas the bottom of the crest of the wave intersects the cutout when the cutout radius is increased to $a = 0.4R$, as shown in Fig. 5. Furthermore, the increase in cutout size affects the location of the node lines and changes the mode shapes as illustrated in the top views of the mode shapes in Fig. 5. Note that, as the cutout size increases, the amplitude of the mode shape near the cutout becomes much higher than the rest of the cylindrical shell.

As shown in Fig. 6, under SS3 boundary conditions, one of the node lines passes through the location of the cutout and the mode shape around the cutout becomes anti-symmetric in the circumferential direction. As also shown in Fig. 6, the mode shapes are not significantly affected by the size of the cutouts for SS3 boundary conditions.

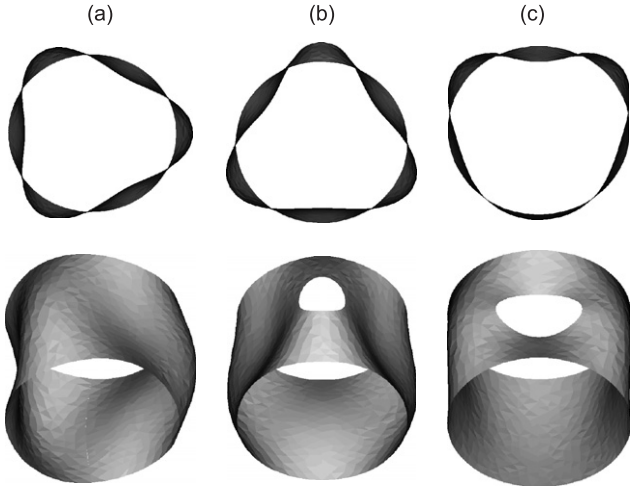

Fig. 5. Selected mode shapes for increasing cutout size for a [90/0/90/0] anti-symmetric cross-ply cylindrical shell under SS2 boundary condition: (a) No cutout, (b) $a/R = 0.2$ and (c) $a/R = 0.4$.

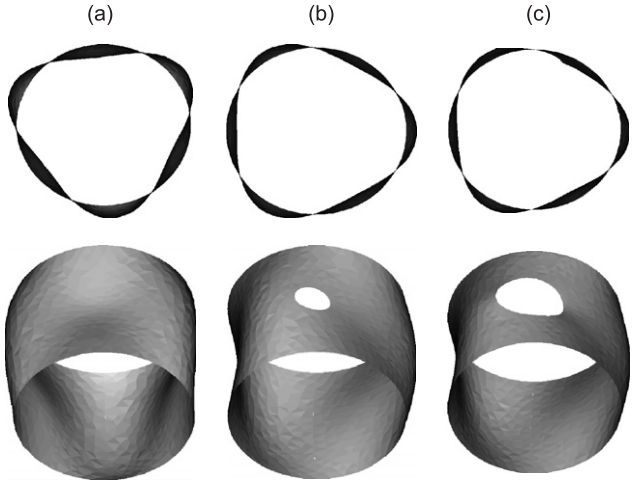

Fig. 6. Selected mode shapes for increasing cutout size for a [90/0/90/0] anti-symmetric cross-ply cylindrical shell under SS3 boundary conditions: (a) No cutout, (b) $a/R = 0.2$ and (c) $a/R = 0.4$.

5.1.2. [90/0/0/90] layup

The natural frequencies of the symmetric cross-ply laminate having a layup of [90/0], under both SS2 and SS3 boundary conditions are shown in Table 3. It is observed that the variation of the natural frequency under SS3 boundary conditions appears to be insignificant. Under SS2 boundary conditions, the natural frequency starts decreasing immediately with the presence of a cutout and experiences a significant change, 7.56% when $a = 0.4R$, from that of a shell without a cutout.

As in the anti-symmetric laminate layup, there exist three waves under both types of boundary conditions. Under SS2 boundary conditions, the mode shape near the cutout is symmetric and remains at the bottom of the crest for $a = 0.2R$, as shown in Fig. 7. For $a = 0.4R$, the cutout remains at the top of the crest in the longitudinal direction and at the bottom of the crest in the circumferential direction, thus forming a saddle-like mode shape. The presence of the cutout alters the locations of the node lines and the mode shapes, as shown in Fig. 7.

Under SS3 boundary conditions, one of the node lines always coincides with the location of the cutout in the longitudinal direction while anti-symmetric mode shapes are observed in the vicinity of the cutout in the circumferential direction for all cases, as shown in Fig. 8. Also, unlike in the case of SS2 boundary conditions, the increase in cutout size has only a local effect on the modal response of the shell while the response away from the cutout is almost intact.

5.2. Effects of a cutout with an increasing shell radius

This case concerns the natural frequency of a shell with a layup of $[45/-45]_{15}$ for increasing shell radius while span length, cutout radius, and shell thickness are specified as $L = 0.1$, $a = 0.005$, and $h = 0.001$,

Table 3
Non-dimensionalized natural frequencies, $\bar{\omega}(= \omega(R^2/h)\sqrt{\rho/E_{22}})$, of a symmetric cross-ply cylindrical shell with increasing cutout size under SS2 and SS3 boundary conditions

Normalized cut-out radius, a/R	$\bar{\omega}$ — Boundary conditions	
	SS2	SS3
0	19.497	20.237
0.1	19.502	20.244
0.2	19.488	20.263
0.3	19.336	20.269
0.4	18.708	20.221

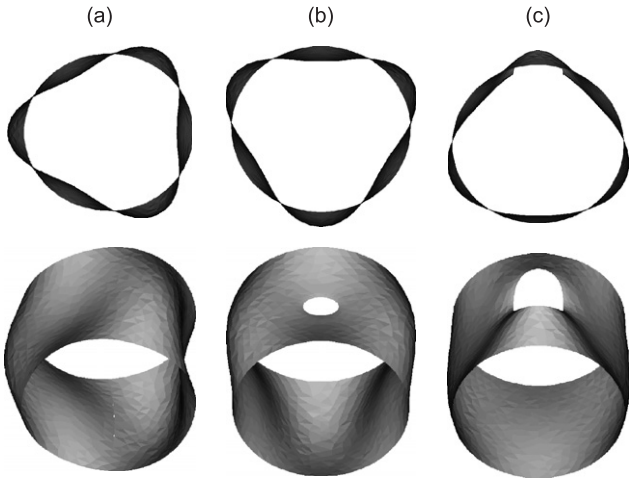

Fig. 7. Selected mode shapes for increasing cutout size for a [90/0/0/90] symmetric cross-ply cylindrical shell under SS2 boundary conditions: (a) No cutout, (b) $a/R = 0.2$ and (c) $a/R = 0.4$.

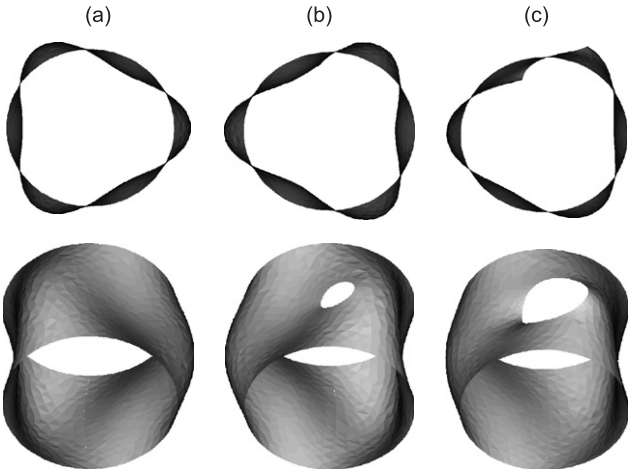

Fig. 8. Selected mode shapes for increasing cutout size for a [90/0/0/90] symmetric cross-ply cylindrical shell under SS3 boundary conditions: (a) No cutout, (b) $a/R = 0.2$ and (c) $a/R = 0.4$.

Table 4
Non-dimensionalized natural frequencies, $\bar{\omega}$ $(= \omega(R_0^2/h)\sqrt{\rho/E_{22}}$, with $R_0 = 0.05)$, of an anti-symmetric angle-ply cylindrical shell with increasing shell radius under SS2 and SS3 boundary conditions

R/a	SS2 boundary conditions		SS3 boundary conditions	
	$\bar{\omega}$ $(a = 0.005)$	$\bar{\omega}$ (no cutout)	$\bar{\omega}$ $(a = 0.005)$	$\bar{\omega}$ (no cutout)
5	22.453	22.686	35.081	35.099
10	18.679	18.728	28.189	28.212
15	16.454	16.465	24.312	24.317
20	15.211	15.213	24.830	24.831
25	14.342	14.342	24.754	24.757

respectively. The shell radius is varied between 5, 10, 15, 20, and 25 times the cutout radius. The natural frequencies under both types of boundary conditions are shown in Table 4. The natural frequency decreases as the shell radius increases for both types of boundary conditions. However, the difference in the natural frequency of the shell with and without a cutout is insignificant for increasing shell radius. The effect of the cutout on the natural frequencies decreases as the shell radius increases.

The mode shapes for $R = 5a$, $15a$, and $25a$ under SS2 boundary conditions are shown in Fig. 9. When the shell radius is five times the cutout radius ($R = 5a$), there exist two waves, and the bottom crest of the wave coincides with the cutout. When the shell radius reaches ten times the cutout radius, ($R = 10a$), the number of waves doubles. As depicted in Fig. 9, the increase in the number of circumferential waves continues with increasing shell radius, and there exist seven waves when the radius of the shell becomes $R = 25a$. For a shell radius of $R = 5a$, the bottom crest of the wave coincides with the cutout location while the top of the crest meets the cutout in the case of $R = 15a$. As for the shell radius of $R = 25a$, the mode shape near the cutout becomes anti-symmetric in the circumferential direction while the node line passes through the cutout in the longitudinal direction. From the top views of the mode shapes shown in Fig. 9, the cutout has almost no effect on the amplitude and shape of the waves around the shell.

Selected mode shapes under SS3 boundary conditions are shown in Fig. 10. For a shell radius of $R = 5a$, there exist three waves, unlike for SS2 boundary conditions. The number of waves becomes five and six when the shell radius is increased to $R = 15a$ and $25a$, respectively. For all shell radii with SS3 boundary conditions, the cutout is always on the side of the wave, i.e., anti-symmetric mode shape and one of the node lines passes

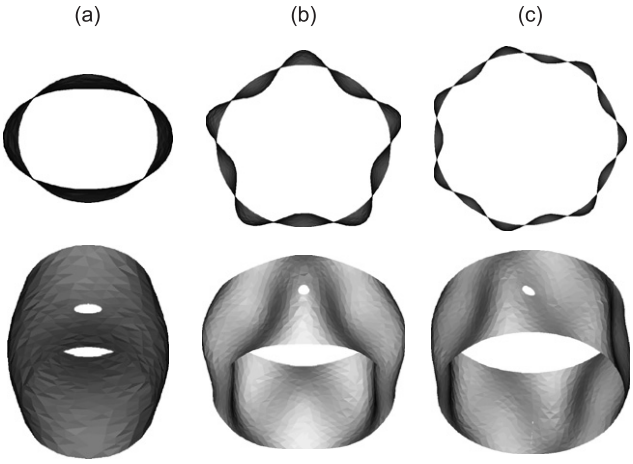

Fig. 9. Selected mode shapes for a $[45/-45]_{15}$ angle-ply cylindrical shell with increasing shell radius under SS2 boundary conditions: (a) $R/a = 5$, (b) $R/a = 15$ and (c) $R/a = 25$.

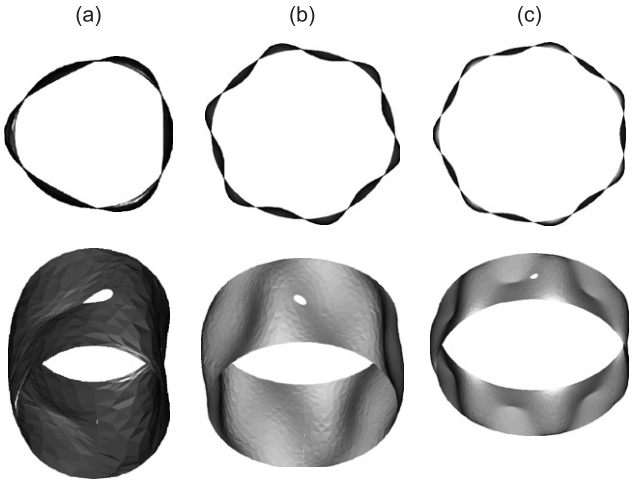

Fig. 10. Selected mode shapes for a $[45/-45]_{15}$ angle-ply cylindrical shell with increasing shell radius under SS3 boundary conditions: (a) $R/a = 5$, (b) $R/a = 15$ and (c) $R/a = 25$.

through the location of the cutout, as shown in Fig. 10. As in the case of SS2 boundary conditions, the cutout has no effect on the amplitude and shape of the waves around the shell.

5.3. *Effects of a cutout with increasing plies*

In order to understand the effect of lamination and shell wall thickness on the vibration response of the cylindrical shell, an anti-symmetric 60-degree, angle-ply laminated shell is considered with varying layups of $[60/-60]_n$ ($n = 1,2,3,4,5$). Hence, the thickness of the shell is increased by considering 2, 4, 6, 8, and 10 plies with equal ply-thicknesses of t. Also, the ply thickness, t, radius of the shell, R, the radius of the cutout, a, and the length of the shell, L, are specified as 0.0015, 0.05, 0.01, and $2R$, respectively.

The natural frequencies under both types of boundary conditions are shown in Table 5. The natural frequency increases as the shell thickness increases for both types of boundary conditions, as expected. However, the difference in the natural frequency of the shell with and without a cutout is insignificant for increasing shell radius under SS3 boundary conditions.

Table 5
Non-dimensionalized natural frequencies, $\bar{\omega}$ ($= \omega(R^2/h_0)\sqrt{\rho/E_{22}}$, with $h_0 = 0.0015$), of an anti-symmetric angle-ply cylindrical shell with increasing number of plies under SS2 and SS3 boundary conditions

No. of layers	SS2 boundary conditions		SS3 boundary conditions	
	$\bar{\omega}$ ($a = 0.01$)	$\bar{\omega}$ (no cutout)	$\bar{\omega}$ ($a = 0.01$)	$\bar{\omega}$ (no cutout)
2	6.436	6.569	10.803	10.802
4	8.970	9.065	14.207	14.215
6	11.051	11.232	16.504	16.508
8	12.289	12.424	19.097	19.140
10	13.714	13.798	21.992	22.086

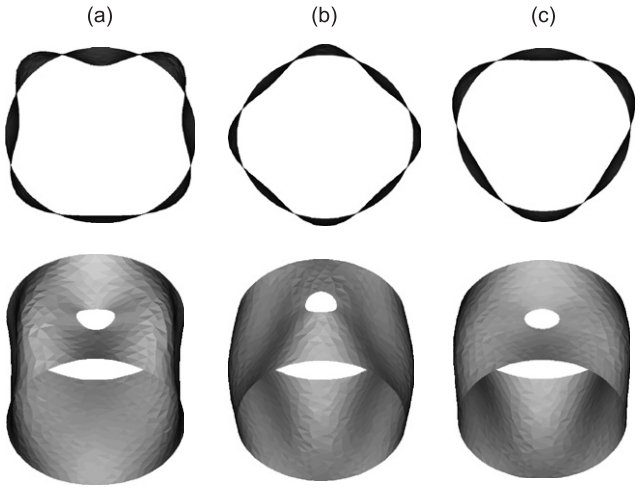

Fig. 11. Selected mode shapes for a [60/−60] angle-ply cylindrical shell with increasing number of plies under SS2 boundary conditions: (a) 2 plies, (b) 4 plies and (c) 10 plies.

Under SS2 boundary conditions, there exist four waves when the shell thickness equals 2 and 4 plies, and three waves when the number of layers is increased to 10. The mode shapes corresponding to the shell thicknesses of 2, 4, and 10 plies under SS2 boundary conditions are illustrated in Fig. 11. As observed in this figure, the cutout intersects the bottom of the wave crest for the 2- and 10-ply laminates, and the top of the crest in the case of the 4-ply laminate. While the modal response is significant near the cutout in the case of the 2-ply laminate, it gradually turns to a uniform pattern of waves around the shell circumference as the number of plies is gradually increased to 10, as shown in the top view of the mode shapes in Fig. 11. This is mainly due to the fact that the material stiffness increases and the material coupling reduces with increasing number of plies in anti-symmetric angle-ply laminates.

Under SS3 boundary conditions, there exist five waves when the shell thickness equals 2 plies and four waves when the shell thickness equals to 6 and 10 plies, as shown in Fig. 12. The reduction in the number of waves is due to the increase in thickness, as also observed under SS2 boundary conditions. Furthermore, one of the node lines always intersects the cutout in the longitudinal direction and the mode shapes around the cutout location are always anti-symmetric in the circumferential direction.

The amplitudes of the waves around the cylindrical shell are the most affected in the case of a 2-ply laminate, as shown in Fig. 12. This is due to the same fact pointed out for SS2 boundary conditions—that the material stiffness increases while the coupling between stretching and twisting decreases with increasing number of plies for anti-symmetric angle-ply laminates, thus resulting in uniform pattern of waves around the cylindrical shell.

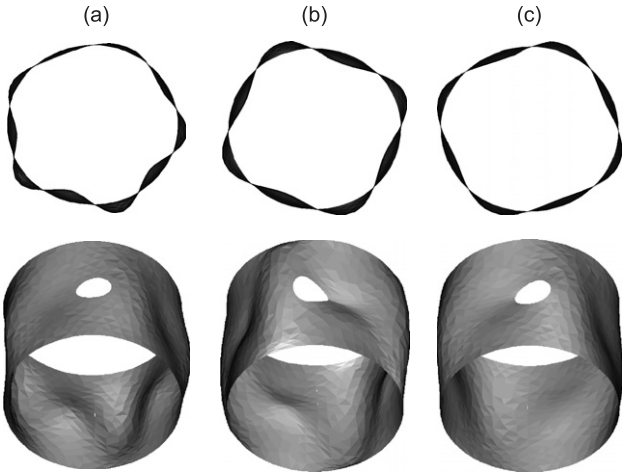

Fig. 12. Selected mode shapes for a [60/−60] angle-ply cylindrical shell with increasing number of plies under SS3 boundary conditions: (a) 2 plies, (b) 6 plies and (c) 10 plies.

6. Conclusions

The effects of a cutout on the natural frequencies and mode shapes were investigated for increasing cutout size, shell radius, and shell thickness. The natural frequencies and mode shapes of cylindrical composite shells responded to a cutout differently, depending on the ply layup and the boundary conditions. The natural frequencies of cylindrical composite shells with SS2 boundary conditions were much more sensitive to the presence of a cutout than shells with SS3 boundary conditions. The mode shapes near the cutout were generally symmetric in both directions under SS2 boundary conditions, whereas the mode shapes around the cutout became anti-symmetric in the circumferential direction and one of the nodes line passed through the cutout in the longitudinal direction under SS3 boundary conditions. When the cutout size was small compared to the radius of the shell, the cutout had little effect on the mode shapes of the shell. Larger cutouts, however, caused a higher response near the cutout than around the rest of the shell, thus significantly affecting the mode shape of the entire cylindrical shell. When the radius of the shell increased but the cutout radius remained the same, the number of circumferential waves increased. This is expected because the circumference of the shell was increasing, resulting in more waves in the circumferential direction. The presence of the cutout did not change the number of circumferential waves for the cases considered. For the layups considered, the natural frequency of the shell with a cutout was always lower than one without a cutout but the effect of a cutout on the natural frequency decreased with increasing shell radius.

Increasing the number of layers for the anti-symmetric angle-ply laminated cylindrical shell caused the stiffness of the shell to increase, thereby increasing the natural frequency and decreasing the number of waves. The presence of the cutout decreased the natural frequency of the shell for the size of the cutout and the laminate layup considered. Furthermore, increasing the number of layers in the anti-symmetric laminate reduced the material coupling effects, thus resulting in more uniform waves around the shell circumference.

References

[1] H.V. Lakshminarayana, K. Dwarakanath, Free vibration characteristics of cylindrical shells made of composite materials, *Journal of Sound and Vibration* 154 (1992) 431–439.

[2] T.C. Ramesh, N. Ganesan, A finite element based on a discrete layer theory for the free vibration analysis of cylindrical shells, *Computers and Structures* 43 (1992) 137–143.

[3] G. Sun, P.N. Bennett, F.W. Williams, An investigation on fundamental frequencies of laminated circular cylinders given by shear deformable finite elements, *Journal of Sound and Vibration* 205 (1997) 265–273.

[4] K.P. Soldatos, On the buckling and vibration of anti-symmetric angle-ply laminated circular shells, *International Journal of Engineering Science* 21 (1983) 217–222.
[5] C. Shu, H. Du, Free vibration analysis of laminated composite cylindrical shells by DQM, *Composites Part B* 28B (1997) 267–274.
[6] X.M. Zhang, Vibration analysis of cross-ply laminated composite cylindrical shells using the wave propagation approach, *Applied Acoustics* 62 (2001) 1221–1228.
[7] F. Moussaoui, R. Benamar, R.G. White, The effects of large vibration amplitudes on the mode shapes and natural frequencies of thin elastic shells. Part II: A new approach for free transverse constrained vibration of cylindrical shells, *Journal of Sound and Vibration* 255 (2002) 931–963.
[8] K.K. Viswanathan, P.V. Navaneethakrishnan, Free vibration study of layered cylindrical shells by collocation with splines, *Journal of Sound and Vibration* 260 (2003) 807–827.
[9] T. Narisawa, A study on refined analytical method for free vibration analysis of laminated composite cylindrical shells using equivalent curvatures, *JSME International Journal* 45 (2002) 32–39.
[10] W. Hufenbach, C. Holste, L. Kroll, Vibration and damping behavior of multi-layered composite cylindrical shells, *Composite Structures* 58 (2002) 165–174.
[11] S. Bicos, G. Springer, Analysis of free damped vibration of laminated composite plates and shells, *International Journal of Solids Structures* 25 (1989) 129–149.
[12] S. Bicos, G.S. Springer, Vibrational characteristics of composite panels with cutouts, *AIAA Journal* 27 (1989) 1116–1122.
[13] H.-T. Hu, J.-Y. Tsai, Maximization of the fundamental frequencies of laminated cylindrical shells with respect to fiber orientations, *Journal of Sound and Vibration* 225 (1999) 723–740.
[14] E. Oterkus, E. Madenci, M. Nemeth, Stress analysis of composite cylindrical shells with an elliptical cutout, *Journal of Mechanics of Materials and Structures* 2 (2007) 695–727.
[15] Netlib Repository, University of Tennessee, Knoxville and Oak Ridge National Laboratory, 〈http://www.netlib.org/eispack/ex/rg.f〉.